PCCP

Accepted Manuscript

ROYAL SOCIETY OF CHEMISTRY

www.rsc.org/pccp

Characterization of Molecular Channel in Photodissociation of $SOCl_2$ at 248 nm: Cl_2 Probing by Cavity Ring-down Absorption Spectroscopy

Bo-Jung Chen, Po-Yu Tsai, Ting-Kang Huang, Zhu-Hong Xia,[a] and King-Chuen Lin*

Department of Chemistry, National Taiwan University, Taipei, and Institute of Atomic and Molecular Sciences, Academia Sinica, Taipei 106, Taiwan

and

Chuei-Jhih Chiou, Bing-Jian Sun, and A. H. H. Chang

Department of Chemistry, National Dong Hwa University, Shoufeng, Hualien 974, Taiwan

Pages: 38
Tables: 2
Figures: 9

***To whom correspondence should be addressed.**
a. On leave from Department of Physics, Southeast University, Nanjing 211189, China.

Abstract

A primary elimination channel of chlorine molecule in one-photon dissociation of $SOCl_2$ at 248 nm is investigated using cavity ring-down absorption spectroscopy (CRDS). By means of spectral simulation, a ratio of vibrational population in the v=0, 1, and 2 levels is evaluated to be 1:(0.10±0.02):(0.009±0.005), corresponding to a Boltzmann vibrational temperature of 340±30 K. The Cl_2 molecular channel is obtained to have a quantum yield of 0.4 ±0.2 from the X^1A' ground state of $SOCl_2$ via internal conversion. The dissociation mechanism differs from a prior study that was reported to obtain a smaller yield <3% initiated from the $2^1A'$ excited state. Temperature-dependence measurements of the Cl_2 fragment turn out to support our mechanism. With the aid of *ab initio* potential energy calculations, two dissociation routes to the molecular products are found, including one synchronous dissociation pathway via a three-center transition state (TS) and the other sequential dissociation pathway via a roaming-mediated isomerization TS. The latter mechanism with a lower energy barrier dominates the dissociation reaction.

I. Introduction

Atmospheric halogen chemistry has drawn much attention, because the emission of halocarbons in troposphere causes severe damage on stratospheric ozone layer. There are several catalytic cycles involving reactive free radicals of Cl, ClO, Br, and BrO that render chlorine and bromine to destroy rapidly the stratospheric ozone.[1-3] The way through UV photodissociation processes may effectively remove these pollutants, because the shortened tropospheric lifetimes of halocarbons essentially prevent transport of these source gases to the stratosphere and thus reduce the amount of reactive free radicals formed. Therefore, understanding the related UV photochemistry is important for the assessment of their environmental impact.

Thionyl chloride ($SOCl_2$) becomes of atmospheric interest, for this molecule may release both Cl and SO; the latter pollutant is readily oxidized to H_2SO_4 as an acid rain source. The photoabsorption and photodissociation of $SOCl_2$ have been well investigated upon irradiation of various photolysis wavelengths,[4-14] especially at 248, 235, and 193 nm. The following three dissociation channels are energetically accessible: (1) SOCl + Cl, (2) SO + Cl_2, and (3) SO + 2Cl, denoted as radical, molecular, and three-body dissociation process, respectively. The prior studies focused on photolysis-wavelength dependence of dissociation channels with the related branch ratio determination,[4-6] anisotropy parameter for each channel that helps evaluate the lifetime and symmetry of the prepared state in the parent molecule, dissociation characterization of the three-body production,[5,6] nascent vibrational and spin-state distributions of SO (ref.4) and determination of spin-orbit states of Cl.[6,10,13] For instance, Weiner and coworkers detected the laser-induced fluorescence of SO upon irradiation of $SOCl_2$ at 193

and 248 nm to characterize three-body fragmentation via either concerted or stepwise process.[4] By using photofragment translational spectroscopy (PTS) at 248 nm, Baum et al. probed the channels Cl_2 + SO and Cl + SOCl which were anticipated to dissociate from initially prepared states with A' and A" symmetry, respectively.[5] The production yield of the former channel was reported to be <3% with the major fragment pair of SO($b^1\Sigma^+$) and Cl_2($X^1\Sigma_g^+$). The yield of three-body fragmentation then reached up to 80% at 193 nm dominating the other channels, all (including molecular channel) resulting from a single potential energy surface (PES).[5] By using a technique of three-dimensional imaging of photofragments, Chichinin et al.[6] probed the resonance-enhanced multi-photon ionization (REMPI) signals of Cl($^2P_{3/2}$) and Cl*($^2P_{1/2}$) (fine-structure ground and excited states denoted as Cl and Cl* thereafter) and their anisotropy parameters. They claimed that the radical and three-body dissociation channels dominate the entire dissociation processes, yielding a branching ratio varied with the photolysis wavelengths. From the previous studies, the fragments of Cl (or Cl*) and SO were detected in order to thoroughly look into the dynamical complexity especially for the channels (1) and (3). Nevertheless, the molecular channel is less stressed, in part because the production yield is little and detection of the fragments becomes less sensitive. This channel was verified by observation of a mass/charge of 70 using PTS at 248 nm.[5] On the contrary, a recent investigation found no evidence of the products of molecular fragmentation using photofragment imaging performed at 235 nm.[6]

Thus far, the Cl_2 fragment has ever been monitored by time-of-flight mass spectrometer,[5] but its optical spectrum has not been observed in order for understanding the internal state distributions. This work aims to probe the optical spectrum of Cl_2 following photolysis of $SOCl_2$ at 248 nm using the cavity

ring-down spectroscopy (CRDS) method. As an important absorption technique, CRDS turns out to be superior to most spectroscopic techniques in detecting the halogen molecules.[15,16] We have recently taken advantage of the CRDS method[16,17] to probe the Br_2 and I_2 fragments in a series of haloalkanes, haloalkenes, and acyl halides. However, it is more challenging to detect Cl_2 fragment, for its absorption cross section in the range of 480 – 520 nm is smaller by two orders of magnitude than the Br_2 molecule. In this work, we attempt to characterize the rovibrational spectrum of Cl_2, confirm the obtained Cl_2 to be a primary product, evaluate the quantum yield of the molecular channel, and elucidate the photodissociation pathway with the aid of theoretical calculations.

II. Experimental

The CRDS apparatus used for photodissociation study is described elsewhere.[18-20] The radiation sources are composed of a 20 ns-pulsed excimer laser emitting at 248 nm for photolysis of $SOCl_2$, and a 5-8 ns-pulsed Nd:YAG laser-pumped dye laser (482-513 nm) used to probe the released Cl_2 fragment in the $B\,^3\Pi_{ou}^+ \leftarrow X\,^1\Sigma_g^+$ transition.[20-22] The intensities of photolysis and probe lasers were controlled in the range of 3-20 and 0.5-1 mJ/pulse, respectively. The photolysis laser beam was focused with a 30-cm focal-length cylindrical lens onto a four-armed stainless steel ring-down cell at a right angle to the cavity, while the probe laser beam was injected along the cavity axis after a 20-30 ns delay. The two beams were overlapped in the center of the flow cell with an overlapping region of (18x1x3)±5 mm^3. The ring-down cell has the long arms sealed by two mirrors with high reflectance of 99.995% at 500 nm, a diameter of 25.4 mm and

a radius of curvature of 1 m. In order to remain mostly the TEM_{00} mode, the probe beam was guided through a spatial filter made of a pair of lenses of 10-cm and 5-cm focal length and a pinhole with 50 μm diameter, prior to injection through the front mirror of the ring-down cell. A photomultiplier tube was positioned behind the rear mirror to detect the intensity of the light pulse leaking out of the mirror. The temporal profile of the ring-down signal was recorded on a transient digitizer. The ring-down time constant for each laser pulse was determined by a best fit to the acquired exponential decay.

The precursors were purified by repeated freeze-pump-thaw cycles at 77 K and then flowed through the ring-down cell at a pressure of 10-200 mTorr monitored by an MKS pressure gauge. The Cl_2 absorption spectra, with a spectral resolution of 0.1 cm^{-1}, were acquired with the aid of a lab-developed program based on a Matlab environment. For the temperature-dependence measurements, the whole chamber was wrapped with copper tubing through which water with constant temperature varied from 280 to 301 K was pumped. The temperature was monitored by a thermocouple positioned nearby the center region.

III. Theoretical methods

A. *Ab initio* electronic structure calculations

As with the work reported for Br_2 previously,[15,18,19] the Cl_2 dissociation channel on the adiabatic ground state PES of $SOCl_2$ is calculated at the level of CCSD/cc-pVTZ. The optimized geometries and the harmonic frequencies of reactant, transition states (TS), and products are obtained at the level of the hybrid density functional theory, B3LYP/cc-pVTZ (transition state ts $SO+Cl_2$ at

MP2/cc-pVTZ); the energies are further refined by the coupled cluster CCSD(T)/cc-pVTZ with B3LYP/cc-pVTZ zero-point energy corrections. The GAUSSIAN09 programs are utilized in the electronic structure calculations.

B. RRKM rate constant calculations

The Rice-Ramsperger-Kassel-Marcus (RRKM) rate constant[23] for Cl_2 dissociations at 248 nm on the singlet ground state PES of $SOCl_2$ is predicted. If the rate of the energy equilibration is faster than the reaction rate, the rate constant can be explained statistically. In addition, provided that total energy is conserved throughout the reaction, the rate constant can be appropriately described by the RRKM theory. In this work, the saddle-point method[23,24] is applied to evaluate the number of states and the density of states; the molecule is viewed as a collection of harmonic oscillators, of which the harmonic frequencies and energy states are obtained as described above.

IV. Results and Discussion

A. Detection of Cl_2 optical spectrum

The absorption spectrum of $SOCl_2$ arises from an origin around 300 nm, yielding two shoulders at 244 and 194 nm with absorption cross section, σ=7.1x10^{-18} and 1.3x10^{-17} cm^2, respectively,[8] that are ascribed to the electronic transitions of (π^*_{SCl}, n_S) and (π^*_{SCl}, n_{Cl}).[7] In this experiment, we applied a photolysis laser beam at 248 nm to excite $SOCl_2$ in the (π^*_{SCl}, n_S) transition, followed by a probe laser beam for detecting the CRDS spectrum of Cl_2 (v=0, 1,

and 2) fragment in the $B^3\Pi_{ou}^+ \leftarrow X^1\Sigma_g^+$ transition at room temperature. When a pair of mirrors with reflectivity of 99.98% were initially installed in the ring-down cell as with detection of the Br_2 spectrum,[18-20] we cannot obtain any Cl_2 signal with significant signal-to-noise ratio. A mirror with higher reflectivity of 99.995% at 500 nm was then installed and the resulting ring-down time of an empty cell was found to extend up to 50 μs. Accordingly, three segments of Cl_2 spectrum were acquired, including the region of 485-487 nm for the transition from the vibrational bands (v',v")=(19-26, 0), 501-503 nm from the bands (12-16, 0) and (18-23, 1), and 511.5-512.5 nm from the bands (9-11, 0), (14-17, 1), and (20-25, 2). An example of the Cl_2(v=0) spectrum is given in Fig.1. The spectral assignment is referred to the report by Coxon.[22,25-27]The Cl_2 memory effect does not exist, because the Cl_2 signals disappear when the photolysis laser is off (Fig.1). A pure Cl_2 spectrum diluted to 5% in Ne buffer gas is also acquired and shown that the spectral region is free from interference of other species.

Three further experiments were conducted in the following in order to verify that the Cl_2 fragment is a primary product upon photodissociation of $SOCl_2$ at 248 nm. The rotational lines at 508.04 nm dominated by P(15) of the (15,1) band and 486.42 nm dominated by P(21) of the (20,0) band were selected for the measurements of laser energy and $SOCl_2$-pressure dependence, respectively. As shown in Fig.2, a plot of rotational intensity as a function of the photolysis laser energy up to 11 mJ/pulse yields a straight line that can be extrapolated through the origin, indicative of a single-photon involvement in the molecular elimination. If an additional photon of 248 nm happens to be successively absorbed into a higher excited state of $SOCl_2$ from which one Cl_2 molecule is eliminated, the energy dependence measurement for such a (1+1)

resonant excitation should yield a slope deviated from unity, unless the second photon absorption is completely saturated. Therefore, this absorption process is minimized. Fig.3 shows a linear plot of the Cl_2 intensity as a function of pressure up to 100 mTorr, beyond which deviation from linearity is found. These experiments confirm that Cl_2 is produced from the photodissociation of a single $SOCl_2$ molecule following absorption of a single photon at 248 nm.

It is of importance to examine the possibility of atomic recombination, because the ring-down time is extended to the μs regime with the current system. To inspect the possibility of Cl_2 resulting from Cl atomic recombination, a single Cl-containing molecule of acetyl chloride (CH_3COCl) is used which has a slightly smaller absorption cross section of 1.15×10^{-19} cm^2,[28] but no Cl_2 signal can be detectable even when the laser energy is increased up to 41 mJ/pulse and the sample pressure enlarged to 800 mTorr, ten times larger than the precursor $SOCl_2$ adopted. This fact indicates that the Cl recombination process is negligible. If the source of Cl atoms is from two separate $SOCl_2$ molecules, then two photons are required for the secondary recombination process. Further, it was reported that a three-body dissociation (SO + Cl + Cl) has no contribution at 248 nm.[5,10] The atomic recombination from this dissociation channel is thus neglected. It usually requires a third body to stabilize the energized Cl_2 product in the reaction, $Cl + Cl \rightarrow Cl_2$, and thus a high pressure environment is necessary. These experimental results may exclude the probable contributions from atomic recombination and secondary reaction of energized fragments.

Is it possible for the eliminated Cl atoms to react with the precursor $SOCl_2$? Rakhymzhan and Chichinin obtained a rate constant k_1 of $(6 \pm 4) \times 10^{-14}$ cm^3/s for the following reaction at 298 K,[29]

$$Cl + SOCl_2 \rightarrow Cl_2 + SOCl . \qquad (1)$$

They also determined the deactivation rate constant of Cl* by $SOCl_2$ to be $(6.2\pm2)\times10^{-12}$ cm^3/s, which was mainly attributed to physical quenching, Cl* + $SOCl_2$ → Cl + $SOCl_2$.[29] A similar case is found in the reactions of $CH_2(\tilde{a}^1A_1)$ and $CH_2(\tilde{X}\,^3B_1)$ with O_2. The depletion rate of $CH_2(\tilde{a}^1A_1)$ by O_2 has been reported to be about 10 times more rapid than that of $CH_2(\tilde{X}\,^3B_1)$.[30-32] However, Hancock and Haverd claimed later that $CH_2(\tilde{a}^1A_1)$ is first quenched by O_2 to the triplet state $CH_2(\tilde{X}\,^3B_1)$, followed by the reaction with O_2 to produce CO_2.[33] The production rate constants of CO_2 from either $CH_2(\tilde{a}^1A_1)$ or $CH_2(\tilde{X}\,^3B_1)$ are essentially the same. Given the pressure of $SOCl_2$ at 100 mTorr, equivalent to 3.5×10^{15} particle/cm^3 at 298 K, and k_1 of $(6\pm4)\times10^{-14}$ cm^3/s, then one Cl atom will lead to one Cl_2 production within 5 ms (eq.1), which is 10^2-10^3 times slower than the ring-down time ~10 μs for the Cl_2 spectral acquisition. If the produced Cl atoms are completely thermalized to room temperature, then the reaction scheme (1) is negligible. However, the Cl atoms gain a kinetic energy up to 106 kJ/mol following photodissociation of $SOCl_2$ at 248 nm. The rate constant k_1 may be enhanced to some extent and the subsequent contribution of Cl_2 from eq.1 becomes possible.

Because the quantum yields of Cl (ref.5) and Cl*(ref.29) in the radical channel were reported to be 96.5% and 52±3% at 248 nm, respectively, a pseudo-first order condition cannot be applied to the reaction scheme (1). The number density of Cl production is estimated in the following under our experimental condition. Given the laser intensity of 10 mJ/pulse which lies in the linear plot of power dependence, the focused area of 18x1 mm^2 by a cylindrical lens, and the absorption cross section of 6.77×10^{-18} cm^2 for $SOCl_2$ at 248 nm that

is determined in the next section, the $SOCl_2$ molecules may dissociate with a rate constant of 0.5/pulse. The resulting Cl atoms eliminated from 100 mTorr $SOCl_2$ give rise to a number density of $0.9x10^{15}$ particle/pulse.cm^3, if the quantum yield of Cl*(or Cl) is 52%. The production of Cl atoms amounts to a factor 0.25 of the number density of $SOCl_2$. For this reason, occurrence of reaction scheme (1) must require two $SOCl_2$ molecules involvement; that is opposed to the pressure-dependence measurement. Even though the Cl_2 product generated from the Cl plus $SOCl_2$ reaction cannot be ruled out, its contribution is limited.

B. Vibrational population and quantum yield of Cl_2 production

To evaluate the Cl_2 vibrational population from the obtained CRDS spectrum cannot rely on the method summing up each rotational line of individual vibrational level, because of the complicated spectral congestion. Instead, we applied spectral simulation method to obtain the vibrational branching for each level. The rotational and vibrational constants of the $^{35}Cl_2$ isotopic variant of the $X\,^1\Sigma_g^+$ and $B\,^3\Pi_{ou}^+$ states have been accurately reported by Coxon.[22,25-27] Due to lack in the literature, the molecular constants of $^{35}Cl^{37}Cl$ and $^{37}Cl^{37}Cl$ are evaluated by means of the isotope ratio.[34] Given those molecular constants, the Cl_2 CRDS spectra may be assigned accurately. The Cl_2(v=0) spectral intensities *I* can be further simulated according to the following equation:

$$I = k\frac{(FCF)(HLF)}{2J^{"}+1}N_{J^{"}}r_{iso}f \qquad \textbf{(2)}$$

where *k* is a factor associated with the instrument and experimental conditions, *FCF* the Franck-Condon factor,[26] *HLF* the Hönl-London factor, *J"* the rotational

quantum number of the ground state Cl_2, $N_{J''}$ the Boltzmann rotational population for which 300 K is assumed, because the rotational population has been thermally equilibrated during a long ring-down time. r_{iso} is the ratio of isotopic variants, $^{35}Cl^{35}Cl$: $^{35}Cl^{37}Cl$: $^{37}Cl^{37}Cl$= 0.57:0.37:0.06. *f* equals 5/3, the intensity ratio of levels with odd and even rotational quantum numbers, because the nuclear spin of Cl is 3/2 and *f* is obtained by (I+1)/I in which I is the nuclear spin quantum number.[34] Note that the nuclear spin of ^{35}Cl and ^{37}Cl are both 3/2, and thus *f* is identical for all isotopic variants. Accordingly, while taking into account all the band transitions involved with the same line width of 0.1 cm^{-1} and the related spectral intensities by eq.2, a spectral simulation for the Cl_2(v=0) population is obtained, appearing consistent with the experimental findings (Fig.1). Then, a theoretical counterpart is analogously obtained in the 501-502 nm range by adjusting the Cl_2(v=1)/Cl_2(v=0) population ratio to be 0.10±0.02 (Fig.4). As the Cl_2(v=1)/Cl_2(v=0) ratio is fixed, a simulated spectrum in the 511.5-512.5 nm region is optimized by adjusting the population ratio of Cl_2(v=2)/Cl_2(v=0) to be 0.009±0.005 (Fig.5). Accordingly, the population ratio of v(0):v(1):v(2) is determined to be 1:(0.10±0.02):(0.009±0.005), accidentally corresponding to a Boltzmann vibrational temperature of 340±30 K.

As reported,[18,20] the quantum yield ϕ of the Cl_2 fragment produced in the 248 nm photolysis of $SOCl_2$ can be evaluated by,

$$\phi = \frac{[Cl_2]}{\frac{E_0}{h\nu\Delta V}(\ell_2 - \ell_1) n\,\sigma} \qquad (3)$$

where $[Cl_2]$ indicates the Cl_2 concentration produced in the beam-crossed region of photolysis/probe lasers, E_o the photolysis laser energy prior to the cell, *h* the Planck's constant, ν the radiation frequency, ΔV the volume of beam-crossed

region, *n* the number density of sample in the cell, σ the absorption cross section of $SOCl_2$ at 248 nm, and ℓ_1 (or ℓ_2) indicates the distance between the inner side of the entrance cell window and the front (or rear) edge of the beam-crossed region. The whole denominator in eq.3 indicates the number of photons absorbed in the beam-crossed region. Because the reflective mirrors are changed, the measurement of Br_2 quantum yield in photolysis of CH_2Br_2 is repeated with the aid of eq.3 to avoid any unknown factor interference and the result is obtained to be 0.21±0.06, consistent with the previous report of 0.2±0.1.[18,35] Due to lack of absorption cross section for high-resolution Cl_2 spectrum, we employed CRDS to determine its value to be 1.27×10^{-21} and 6.50×10^{-22} cm^2 at 501.89 and 508.04 nm, respectively, as shown in Fig.6. The obtained results are smaller by two order of magnitude than the Br_2 molecule which has a σ of 1.3×10^{-19} cm^2 at 519.68 nm.[36] As with the measurements conducted in CH_2Br_2, the Cl_2 concentration at 508.04 nm and the photon numbers absorbed in the beam-crossed region were evaluated directly to yield ϕ of 0.40±0.13 for the Cl_2 dissociation channel.

For confirming the direct measurement of ϕ based on eq.3 is reliable, we proceeded alternatively via an indirect measurement using a sample with known ϕ as a reference. In this manner, the quantum yield of Cl_2 in photolysis of $SOCl_2$ was determined by comparing with that of Br_2 in CH_2Br_2 as a reference sample. Then, the following formula is obtained from eq.3,

$$\frac{\phi_s}{\phi_r} = \frac{[Cl_2]}{\sigma_s E_s n_s} / \frac{[Br_2]}{\sigma_r E_r n_r} \qquad (4)$$

where the subscript s and r denote $SOCl_2$ and CH_2Br_2, respectively, E, the photolysis laser energy for parent molecule, and n, the number density in the cell. The absorption cross section σ_r of CH_2Br_2 was reported to be $(3.36\pm0.08)\times10^{-19}$ cm^2,[37] and $SOCl_2$ was determined to be $(6.77\pm0.34)\times10^{-18}$ cm^2 at 248 nm in a

10-cm long gas cell using a UV/Vis absorption spectrometer, consistent with a previous result of 7.05×10^{-18} cm^2.[8] To improve the accuracy, three reference samples of acetyl bromide, acetyl chloride, and acetone with known σ of 2.43×10^{-19} (ref.38), 1.15×10^{-19} (ref.28), and 2.20×10^{-20} cm^2 (ref.39), respectively, were adopted to calibrate the instrument factor. Given the quantum yield of Br_2 produced by CH_2Br_2 at 248 nm, the absorption cross section of Cl_2 and Br_2 at related wavelengths, the photolysis laser energies and pressures adopted each for $SOCl_2$ and CH_2Br_2, along with the individual measurements of a relative line intensity of Br_2 at 519.68 nm and Cl_2 at 501.89 or 508.04 nm, respectively, the Cl_2 quantum yield was thus obtained to be 0.4±0.2, in agreement with that determined directly. Despite two methods adopted differently, they are essentially originated from the same formula (eq.3) and cannot be considered to be independent of each other.

Given the pressure of $SOCl_2$ at 100 mTorr in the ring-down cell, collision cross section assumed to be 50 $Å^2$ between Cl_2 and other partners, and an upper limit of relative speed of 500 m/s for the colliders, the mean free path is estimated to be ~0.4 mm and the subsequent diffusion coefficient is about 7×10^{-2} m^2/s. The root-mean-squared distance that the Cl_2 molecules diffuse within a detection period of 20-30 μs ring-down time is about 1 mm, which is confined within the cross section (diameter =3 mm) along the detection axis. In addition, upon the photolysis, the instant pressure in the interactive volume increases largely (>100 mTorr) such that the Cl_2 diffusion is further slowed down. Thus, the diffusion effect of the Cl_2 molecules that might cause the signal decay and the probable redistribution of translational and internal energies should be minimized.

C. Photodissociation mechanism

As shown in Fig.7, the ab initio potential energy calculations for the photodissociation of $SOCl_2$ lead to the products SO + Cl_2, SOCl + Cl, and SCl_2 + O. However, the last channel requires the dissociation energy of about 500 kJ/mol that exceeds the excitation energy set at 482.3 kJ/mol equivalent to the wavelength 248 nm. Some related geometric structures of reactant, TSs and products are depicted in Fig.8 and the detailed energy states are listed in Table I. There are two pathways leading to the molecular channel, Cl_2 + SO. One route is via a three-center TS with two S-Cl bonds prolonged almost identically from 2.130 to 2.603 Å lying at 379.6 kJ/mol with respect to the ground state $SOCl_2(^1A')$. The dissociation rate constant for the synchronous dissociation pathway is evaluated to be $4.81x10^{10}$ s^{-1}. The other route is via an isomerization TS. In such a sequential photodissociation mechanism, a single S-Cl bond breaks first, and then the released Cl atom moves to form a Cl-Cl bond in the isomerization TS, followed by the Cl_2 elimination. The corresponding rate constant is about $8.72x10^{11}$ s^{-1}, as restricted by the rate determining step, $SOCl_2(^1A') \rightarrow\rightarrow ts_{SO+Cl2}$ (roaming) lying at 281.2 kJ/mol. The related rate constants evaluated by the RRKM method are listed in Table II. The sequential photodissociation mechanism tends to dominate the dissociation processes, for its rate constant is about 20 times larger than the other route. By analogy, the route via such an isomerization TS was reported to dominate the molecular products for multi-halocarbons such as CF_2Cl_2, CF_2Br_2, and $CHBr_3$.[40] For instance, in an infrared multiphoton dissociation of CF_2Cl_2, a quantum yield ~10% of Cl_2 elimination has been observed by Lee and coworkers.[41] The decomposition via isomerization TS $CF_2Cl\cdots Cl$ was anticipated to be the key pathway to this molecular product, yielding a 3% of the Cl_2 yield in appreciable agreement with

the observation.[40] Such a roaming-mediated isomerization pathway was also found in such as nitrobenzene[42] and nitromethane[43,44] to account for a significant yield of the NO elimination. For instance, Suits, Bowmen and coworkers[45] carried out infrared multiphoton dissociation of nitromethane to examine this unimolecular decomposition near threshold. They found that the roaming-mediated isomerization pathway dominates the NO loss channel, yielding a small translational energy release and a feature of the Λ-doublet propensity of NO, favoring an unpaired electron lying in the pπ orbital perpendicular to the plane of rotation. The other roaming signature is that the methothy co-product is vibrationally excited. We expect that the roaming-mediated isomerization pathway found in $SOCl_2$ might carry a similar feature.

To confirm the dissociation pathway mainly initiated on the energetic ground state, temperature dependence of Cl_2 product is examined. The rotational line at 486.42 nm was selected for these measurements. As shown in Fig.9, given $SOCl_2$ at a pressure of 60 mTorr, the Cl_2 yield is enhanced by 16% within the temperature increment from 287 to 301 K. As the temperature increases, higher levels of excited state are populated such that the increased density of states may enhance the total rate of level-to-level coupling and make the process of internal conversion (IC) more efficient. When temperature was further extended, the increased vapor pressure of the precursor went beyond the linear range of the pressure dependence (Fig.3). In Baum et al experiments with molecular beam apparatus under jet-cooled temperature,[5] the low temperature condition allows for only a narrow population spread in the ground and the subsequent excited electronic state such that the IC process via the level-to-level coupling is less efficient. In contrast, the precursor contained in the ring-down cell at ~300 K has

chance to populate in different vibrational modes and levels of the excited state upon the laser irradiation. Different vibrational modes and levels result in different molecular symmetric properties which can dramatically change the dissociation efficiency. In the isomerization reaction of vinylidiene ($H_2C=C$)→ acetylene (HCCH), the lifetimes of vinylidiene were calculated to vary from 10^{-2} to 60 ps depending on excitation of selected vibrational mode.[46,47] Therefore, when precursor is populated in some vibrational modes with slowed predissociation processes, the IC has chance to give rise to new dissociation fragments. For instance, in the 248 nm photodissociation of the C_2H_5COCl molecular beam heated to 153 ^{0}C, the major fast dissociation channel of C–Cl bond fission in the picosecond regime was accompanied by a minor channel of HCl elimination which proceeded on the ground state.[48] In contrast, the HCl elimination was not observed in a supersonic molecular beam at cold temperature.[49]

In view of the measurements of Cl_2 at m/z = 70 and its anisotropy parameter of 0.7±0.1 using PTS, Baum et al.[5] have proposed that the molecular products mainly $SO(b^1\Sigma^+)$ + $Cl_2(X^1\Sigma_g^+)$, contributing only <3% of the entire decay process, are dissociated from the prepared 2^1A' state with a decay lifetime comparable to the rotational period or even shorter. In contrast, the predominant dissociation process is found to proceed via the fast ($<10^{-12}$s) radical channel SOCl + Cl that results from the 2^1A" state. Chichinin et al. recently calculated the oscillator strengths of the electronically excited singlet states, obtaining 2A' and 2A" to be 0.024 and 0.009, respectively, with some uncertainty.[6] In light of comparison of their oscillator strengths, it is surprising to find such a small yield for the molecular channel. They thus anticipated that the 2^1A' state may not be repulsive with respect to the 2^1A" state such that IC or

intersystem crossing are allowed to occur significantly.

Different from the dissociation route reported previously,[5] we believe that the primary Cl_2 fragment in molecular channel observed in this work is dissociated on the $\tilde{X}\,^1$A' ground state surface via IC that is facilitated by the efficient 2^1A'- $\tilde{X}\,^1$A' coupling. If the molecular channel proceeds rapidly from the excited state, then the Cl_2 fragment may not be sensitive to the temperature effect, since the further increased amount of $SOCl_2$ after 300 K does not have enough time to quench the excited molecules that lead to the Cl_2 production channel. For instance, given 500 mTorr of $SOCl_2$ corresponding to a number density of $2x10^{16}$ molecules/cm^3, an upper limit of relative speed about 10^5 cm/s at much higher temperature than 300 K, and the collision cross section assumed to be 50 $Å^2$, each excited $SOCl_2$ molecule may encounter $1x10^{-5}$ collisions during the rotational period of ~1 ps. Therefore, if the molecular dissociation lifetime of the prepared 2^1A' state is comparable to the rotational period, the excited state molecules will not suffer from collision quenching by the temperature increment. In contrast, the excited state population encounters a collision number of ~10^2 during a ring-down time of 10 μs, thereby facilitating the process of collision-induced internal conversion.

According to the theoretical pathway calculations, the main route is via a tsOSCl-Cl at 269.1 kJ/mol, followed by an isomerization TS at 281.2 kJ/mol with a structure SOCl…Cl, (Fig.8) in which the Cl..Cl distance of 2.057Å is close to the bond length 2.024 Å of the ground state Cl_2. That is one of the reasons why the vibrational temperature of Cl_2 appears as low as about 340±30 K. The other reason may be caused by the effect of vibrational near-resonance energy transfer within the long ring-down time. The $SOCl_2$ structure contains two SCl_2 stretching modes of symmetric ν_2 (492 cm^{-1}) and anti-symmetric ν_5 (455 cm^{-1})[50]

which are close to the $Cl_2(X^1\Sigma_g^+)$ harmonic frequency of 559.7cm^{-1}.[25] Thus, the large internal energy of $Cl_2(v)$ has a chance to efficiently transfer to $SOCl_2$.

While looking into the isomerization TS structure, the OS..ClCl is prolonged to 2.552 Å such that SO and Cl_2 may break up easily. This route may well be related to a roaming mechanism, in which the released Cl atom meanders in a near flat potential energy surface formed by Cl +SOCl and finally abstract another Cl atom forming SO and Cl_2, as with the roaming route found in H_2CO.[51-55]

V. Conclusion

By using cavity ring-down absorption spectroscopy, we have characterized the optical spectrum of Cl_2 fragment resulting from a molecular channel mainly composed of $SO(b^1\Sigma^+)$ and $Cl_2(X^1\Sigma_g^+)$ in one-photon photolysis of $SOCl_2$ at 248 nm. It is more difficult to detect Cl_2 fragment, as compared to the Br_2 and I_2 cases, since the former bears an absorption cross section about two orders of magnitude smaller. Despite a longer ring-down time of 10 μs, the obtained primary Cl_2 fragment has been carefully inspected to rule out the possibility of Cl atomic recombination and secondary reaction of energized fragments. The Cl_2 contribution from the reaction between Cl and precursor is also minimized.

The CRDS spectrum of Cl_2 has been analyzed by means of spectrum simulation to evaluate the ratio of vibrational population at v=0, 1 and 2 which is equal to 1:(0.10±0.02):(0.009±0.005), corresponding to a Boltzmann vibrational temperature of 340±30 K. As reported previously, the molecular channel with a small yield <3% was found to result rapidly from the $2^1A'$ excited state of $SOCl_2$. Different from the reported pathway, the Cl_2 product that is determined to have

a quantum yield of 0.4 ±0.2 is dissociated on the $\tilde{X}$ ^{1}A' ground state surface via internal conversion. Temperature-dependence measurements of the Cl_2 fragment help support the proposed mechanism. Further, with the aid of *ab initio* potential energy calculations, two probable routes to the molecular products are suggested, including one synchronous dissociation pathway via a three-center TS and the other sequential dissociation pathway via an isomerization TS. The latter mechanism with a lower energy barrier dominates the decay reaction. This route may well be related to a roaming mechanism, in which the released Cl atom moves in a weakly attractive potential energy surface formed by moieties and finally abstracts another Cl atom forming SO and Cl_2.

Acknowledgments

This work is supported by Ministry of Science and Technology of Taiwan, Republic of China under contract no. NSC 99-2113-M-001-025-MY3. Computer resources at the National Center for High-performance Computer of Taiwan were utilized in the calculations.

References

1. M. J. Molina and F. S. Rowland, Nature **249**, 810 (1974).
2. J. Farman, B. Gardiner, and J. Shanklin, Nature **315**, 207 (1985).
3. S. A. Montzka, J. H. Butler, R. C. Myers, T. M. Thompson, T. H. Swanson, A. D. Clarke, L. T. Lock, and J. W. Elkins, Science **272**, 1318 (1996).
4. H. Wang, X. Chen, and B. R. Weiner, J. Phys. Chem. **97**, 12260 (1993).
5. G. Baum, C. S. Effenhauser, P. Felder, J. R. Huber, J. Phys. Chem. **96**, 756 (1992).
6. A. Chichinin, T. S. Einfeld, K. H. Gericke, and J. Grunenberg, Phys. Chem. Chem. Phys. **7**, 301 (2005).
7. M. Kawasaki, K. Kasatani, H. Sato, H. Shinohara, N. Nishi, H. Ohtoshi, and I. Tanaka, Chem. Phys. **91**, 285 (1984).
8. A. P. Uthmann, P. J. Demlein, T. D. Aliston, M. C. Withiam, M. J. McClements, and G. A. Takacs, J. Phys. Chem. **82**, 2252 (1978).
9. C. Maul and K.-H. Gericke, Int. Rev. Phys. Chem. **16**, 1 (1997).
10. M. Roth, C. Maul, and K.-H. Gericke, Phys. Chem. Chem. Phys. **4**, 2932 (2002).
11. E. A. J. Wannenmacher,P. Felder, and J. R. Huber, J. Chem. Phys. **95**, 986 (1991).
12. R. J. Donovan, D. Husain and P. T. Jackson, Trans. Faraday Soc. **65**, 2930 (1969).
13. M. Kawasaki, K. Suto, Y. Sato, Y. Matsumi and R. Bersohn, J. Phys. Chem. **100**, 19853 (1996).
14. H. Okabe, J. Chem. Phys. **56**, 3378 (1972).
15. H. Fan, P. Y. Tsai, K. C. Lin, C. W. Lin, C.Y. Yan, S.W. Yang, and A. H. H.

Chang, J. Chem. Phys.**137**, 214304 (2012).

16. K. C. Lin and P. Y. Tsai, Phys. Chem. Chem. Phys. **16**, 7184 (2014).
17. J. J. Scherer, J. B. Paul, A. O'Keefe, and R. J. Saykally, Chem. Rev. **97**, 25 (1997).
18. P. Y. Wei, Y. P. Chang, Y. S. Lee, W. B. Lee, K. C. Lin, K. T. Chen, and A. H. H. Chang, J. Chem. Phys. **126**, 034311 (2007).
19. H. L. Lee, P. C. Lee, P. Y. Tsai, K. C. Lin, H. H. Kuo, P. H. Chen, and A. H. H. Chang, J. Chem. Phys. **130**, 184308 (2009)
20. C. C. Wu, H. C. Lin, Y. B. Chang, P. Y. Tsai, Y. Y. Yeh, H. Fan, K. C. Lin, and J. S. Francisco, J. Chem. Phys. **135**, 234308 (2012).
21. Laboratoire Aime Cotton, http://www.lac.u-psud.fr/-Atlas-de-l-iode-et-du-tellure-
22. J. A. Coxon and R. J. Shanker, J. Mol. Spectrosc. **69**, 109 (1978).
23. A. H. H. Chang, A. M. Mebel, X. M. Yang, S. H. Lin, and Y. T. Lee, J. Chem. Phys. **109**, 2748 (1998).
24. H. Eyring, S. H. Lin, and S. M. Lin, *Basic Chemical Kinetics* (Wiley, New York, 1980).
25. M. A. A. Clyne, and J. A. Coxon, J. Mol. Spectrosc. **33**, 381 (1970)
26. J. A. Coxon, J. Quant. Spectrosc. Radiat. Transfer. **11**, 1355 (1971).
27. J. A. Coxon, J. Mol. Spectrosc. **82**, 264 (1980).
28. G. Libuda, F. Zabel, and K. H. Becker, *Step-Halocside/Afeas Workshop on Kinetics and Mechanisms for the Reactions of Halogenated Organic Compounds in the Troposphere, Dublin, Ireland, May 1991.*
29. A. Rakhymzhan and A. Chichinin, J. Phys. Chem. A **114***,* 6586(2010).
30. T. Bohland, F. Temps, H.Gg. Wagner, Ber. Bunsenges. Phys. Chem. **88**, 455 (1984).

31.D.C. Darwin, A.T. Young, H.S. Johnston, and C.B. Moore, J. Phys. Chem. **93**, 1074(1989)

32. U. Bley, F. Temps, H.Gg. Wagner, and M. Wolf, Ber. Bunsenges. Phys. Chem. **96**, 1043 (1992).

33. G. Hancock and V. Haverd, Chem. Phys. Lett. **372**, 288(2003).

34. G. Herzberg, *Molecular Spectra and Molecular Structure: Spectra of Diatomic Molecules* (Krieger Pub Co, 2 edition, 1989).

35. P. Y. Wei, Y. P. Chang, W. B. Lee, Z. Hu, H. Y. Huang, K. C. Lin, T. K. Chen, and A. H. H. Chang, J. Chem. Phys. **125**, 133319 (2006).

36.H. Y. Huang, W. T. Chuang, R. C. Sharma, C. Y. Hsu, K. C. Lin, and C. H. Hu, J. Chem. Phys. **121**, 5253 (2004).

37.J. C. Mossinger, D. E. Shallcross, and R. A. Cox, J. Chem. Soc., Faraday Trans. **94**, 1391 (1998).

38. V. Khamaganov, R. Karunanandan, A. Rodriguez, and J. N. Crowley, Phys. Chem. Chem. Phys. **9**, 4098 (2007).

39. R. Atkinson, D. L. Baulch, R. A. Cox, J. N. Crowley, R. F. Hampson R. G. G. Hynes, M. E. Jenkin, M. J. Rossi, and J. Troe, Atmos. Chem. Phys. **6**, 3625 (2006).

40. A. Kalume, L. George, and S. A. Reid, J. Phys. Chem. Lett. **1**, 3090 (2010).

41. D. Krajnovich, F. Huisken, Z. Zhang, Y. R. Shen, and Y. T. Lee, J. Chem. Phys. **77**, 5977 (1982).

42. M. L. Hause, N. Herath, R. Zhu, M. C. Lin, and A. G. Suits, Nat. Chem. **3**, 932 (2011).

43. Z. Homayoon, J. M. Bowman, A. Dey, C. Abeysekera, R. Fernando, and A. G. Suits, Z. Phys. Chem. **227**, 1267 (2013).

44. Z. Homayoon and J. M. Bowman, J. Phys. Chem. A **117**, 11665 (2013).

45. A. Dey, R. Fernando, C. Abeysekera, Z. Homayoon, J. M. Bowman, and A. G. Suits, J. Chem. Phys. **140**, 054305 (2014).

46. T. Carrington, Jr., L. M. Hubbard, H. F. Schaefer III, and W. H. Miller, J. Chem. Phys. **80**, 4347 (1984).

47. B. Li and W. Bian, J. Chem. Phys. **129**, 024111 (2008).

48. L. R. McCunn, M. J. Krisch, K. Takematsu, L. J. Butler, and J. N. Shu, J. Phys. Chem. A **108**, 7889 (2004)..

49. Z. R. Wei, X. P. Zhang, W. B. Lee, B. Zhang, and K. C. Lin, J. Chem. Phys. **130**, 014307 (2009).

50.T. Shimanouchi, J. Phys. Chem. Ref. Data, **6**, 993(1972).

51.D. Townsend, S. A. Lahankar, S. K. Lee, S. D. Chambreau, A. G. Suits, X. Zhang, J. Rheinecker, L. B. Harding, and J. M. Bowman, Science **306**, 1158 (2004).

52. A. G. Suits, Acc. Chem. Res. **41**, 873 (2008).

53. S. A. Lahankar, S. D. Chambreau, D. Townsend, D. Suits, J. Farnum, X. Zhang, J. M. Bowman, and A. G. Suits, J. Chem. Phys. **125**, 044303 (2006).

54. S. A. Lahankar, S. D. Chambreau, X. Zhang, J. M. Bowman, and A. G. Suits, J. Chem. Phys. **126**, 044314 (2007).

55. S. A. Lahankar, V. Goncharov, F. Suits, J. D. Farnum, J. M. Bowman, and A. G. Suits, Chem. Phys. **347**, 288 (2008).

Table I. The calculated energies for the reactants, intermediates, transition states, and dissociation products for the Cl, Cl_2, SO, SCl_2, SOCl dissociation channels on the adiabatic singlet ground state potential energy surface of $SOCl_2$.

	B3LYP/ cc-pVTZ + E_{zpc} [a]	E_{zpc} [b]	[c]CCSD/ cc-pVTZ	E(kJ/mol)[d]	E(kJ/mol)[e]
$SOCl_2$	-1393.922362	0.006705	-1392.258130	0.0	0.0
SO	-473.378052	0.002615	-472.750484		
SOCl	-933.678013	0.004372	-932.527156		
Cl	-460.174664	0.000000	-459.666282		
Cl_2	-920.434019	0.001225	-919.409113		
O(triplet)	-75.091864	0.000000	-74.971050		
O(singlet)	-74.990250	0.000000	-74.882416		
SCl_2(singlet)	-1318.678155	0.002726	-1317.152936		
SCl_2(triplet)	-1318.638906	0.001919	-1317.096911		
SO+Cl_2	-1393.812071	0.003840	-1392.159597	289.6	251.2
SOCl+Cl	-1393.852677	0.004372	-1392.193437	183.0	163.7
SCl_2+O(singlet)	-1393.668405	0.002726	-1392.035352	666.8	574.5
SCl_2+O(triplet)	-1393.730770	0.001919	-1392.067962	503.0	486.7
OSCl-Cl	-1393.848438	0.005684	-1392.165697	194.1	240.0
SO+2Cl	-1393.727380	0.002615	-1392.083047	511.9	448.9
SOCl-Cl	-1393.815219	0.004533	-1392.162226	281.3	246.1
$ts_{OSCl-Cl}$	-1393.838018	0.005375	-1392.154322	221.4	269.1
$ts_{SOCl-Cl}$	-1393.813031	0.004058	-1392.161473	287.0	246.8
ts_{SO+Cl2} (conventional)[f]	-1392.062513	0.004629	-1392.111478		379.6
ts_{SO+Cl2} (roaming)[f]	-1392.116469	0.004020	-1392.148332		281.2

[a] B3LYP/cc-pVTZ energy with zero-point energy correction in hartree

[b] zero-point energy by B3LYP/cc-pVTZ in hartree

[c] CCSD/cc-pVTZ energy with zero-point energy correction in hartree.

[d] relative energy by B3LYP/cc-pVTZ with zero-point energy correction

[e] relative energy by CCSD/cc-pVTZ with B3LYP/cc-pVTZ zero-point energy correction

[f] geometry optimized by MP2/cc-pVTZ

Table II. RRKM rate constants computed with B3LYP/cc-pVTZ zero-point energy corrected CCSD/cc-pVTZ energies and B3LYP/cc-pVTZ harmonic frequencies for reactions paths on the adiabatic singlet ground state surface of $SOCl_2$ at 248 nm.

	248 nm ($SOCl_2$)
$^{a}k_1$ ($SOCl_2 \rightarrow SO+Cl_2$)	4.81×10^{10} s^{-1}
k_2 ($SOCl_2 \rightarrow$ OSCl-Cl)	1.28×10^{12} s^{-1}
k_{-2} (OSCl-Cl $\rightarrow SOCl_2$)	2.62×10^{12} s^{-1}
k_3 (OSCl-Cl $\rightarrow$ SOCl-Cl)	6.41×10^{14} s^{-1}
k_{-3} (SOCl-Cl $\rightarrow$ OSCl-Cl)	2.71×10^{13} s^{-1}
$^{a}k_R$ (SOCl-Cl $\rightarrow SO+Cl_2$)	8.72×10^{11} s^{-1}

[a] transition state optimization by MP2/cc-pVTZ.

Figure Captions

Fig.1 A portion of Cl_2 spectra acquired in the photolysis of $SOCl_2$ at 248 nm. (a) the background spectrum obtained without irradiation of 248nm, (b) Cl_2(v=0) spectrum acquired experimentally, (c) the spectrum of 5% Cl_2 in Ne buffer gas containing the v=0 band, and (d) spectral simulation taking into account all the isotopic variants of $^{35}Cl_2$ $^{35,37}Cl_2$, and $^{37}Cl_2$. Partial assignments are added, including the $B^3\Pi_{ou}^+$ (v'=20 and 21) ← $X^1\Sigma_g^+$ (v"=0 and 0) transitions.

Fig.2 Laser energy dependence of Cl_2 fragment intensity at 508.04 nm contributed mainly from the rotational line P(15) of the (15,1) band. $\Delta(1/\tau)$ denotes difference of the reciprocal of ring-down time with and without precursor in photolysis.

Fig.3 Cl_2 fragment intensity as a function of the $SOCl_2$ pressure within 100 mTorr. The rotational line at 486.42 nm is selected for the measurements.

Fig.4 A portion of Cl_2 spectra in the range of 501-502.1 nm acquired in the photolysis of $SOCl_2$ at 248 nm. (a) trace acquired experimentally for the bands of v=0 and 1, (b) the simulated counterpart with a population ratio of v(0)/v(1) equal to 1/(0.10±0.02). Partial assignments are added, including the $B^3\Pi_{ou}^+$ (v'=13 and 18) ← $X^1\Sigma_g^+$ (v"=0 and 1) transitions.

Fig.5 A portion of Cl_2 spectra in the range of 511.7-512.7 nm acquired in the photolysis of $SOCl_2$ at 248 nm. (a) trace acquired experimentally for the bands of v=0, 1, and 2, (b) the simulated counterpart with a population ratio of v=0, 1, and 2 equal to 1:(0.10±0.02):(0.009±0.005), corresponding to vibrational temperature 340±30 K. Partial assignments are added,

including the $B^3\Pi_{ou}^+$ (v'=10, 14 and 21) ← $X^1\Sigma_g^+$ (v"=0, 1 and 2) transitions.

Fig.6 Absorption cross section measured for high-resolution spectrum of Cl_2 prepared in a 20% in Ne buffer gas. Partial assignments are added, including the $B^3\Pi_{ou}^+$ (v'=13 and 18) ← $X^1\Sigma_g^+$ (v"=0 and 1) transitions.

Fig.7 The dissociation pathways of $SOCl_2$ leading to Cl_2 + SO, in units of kJ/mol relative to the ground state, are computed with CCSD(T)/cc-pVTZ level of theory with B3LYP/cc-pVTZ zero-point energy corrections at B3LYP/cc-pVTZ optimized geometries. Two dissociation routes are expected, including one via a three-center transition state (TS) at 379.6 kJ/mol and the other via a roaming-mediated isomerization TS at 281.2 kJ/mol. For those pathways with dashed lines, the attempts for locating the transition states are not made or not successful.

Fig.8 The related structures along the dissociation pathway of $SOCl_2$.

Fig.9 Temperature dependence of the Cl_2 line intensity at 486.42 nm in photodissociation of $SOCl_2$ at 248 nm. Photolysis laser energy was fixed at 8 mJ and sample pressure was at 60 mTorr.

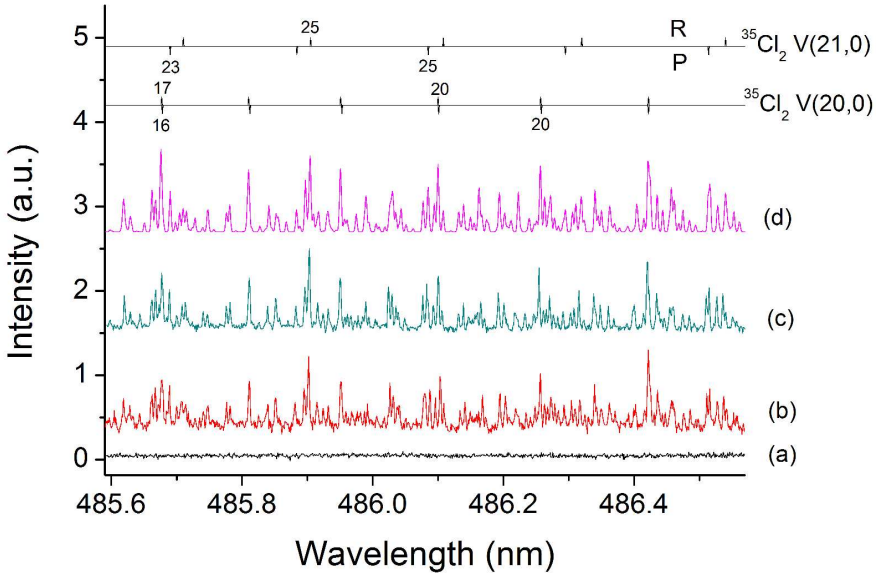

Fig.1

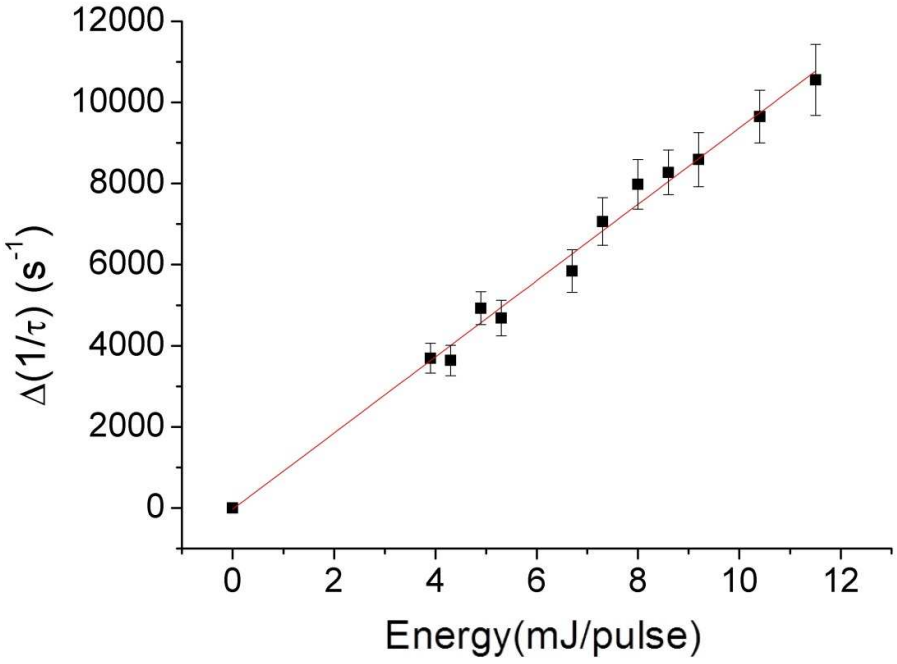

Fig.2

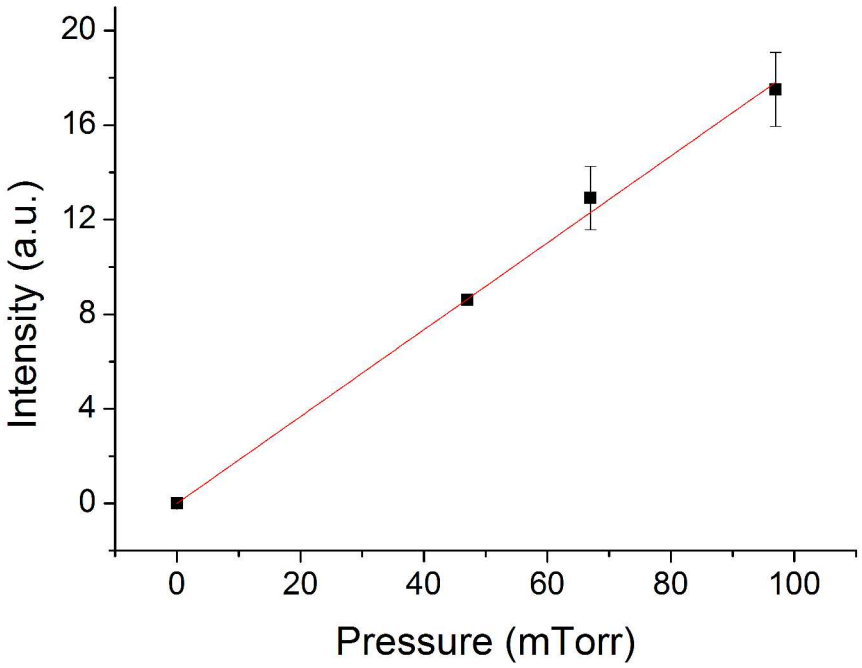

Fig.3

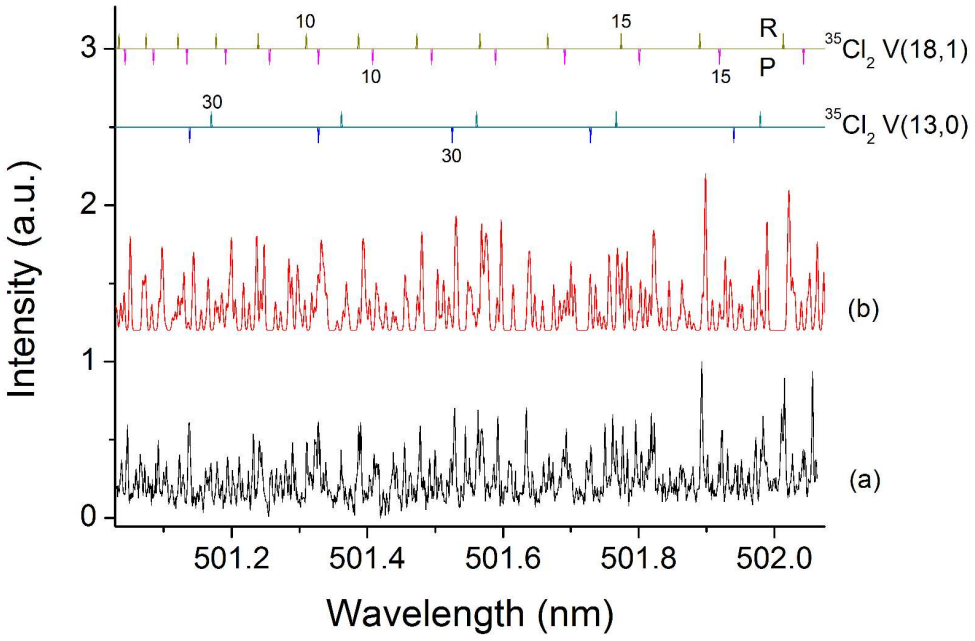

Fig.4

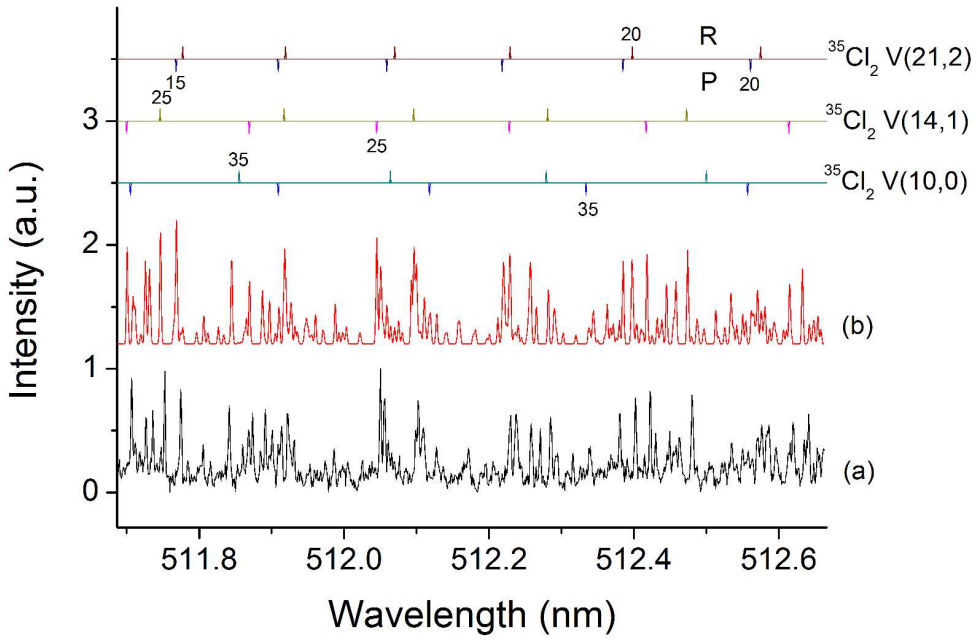

Fig.5

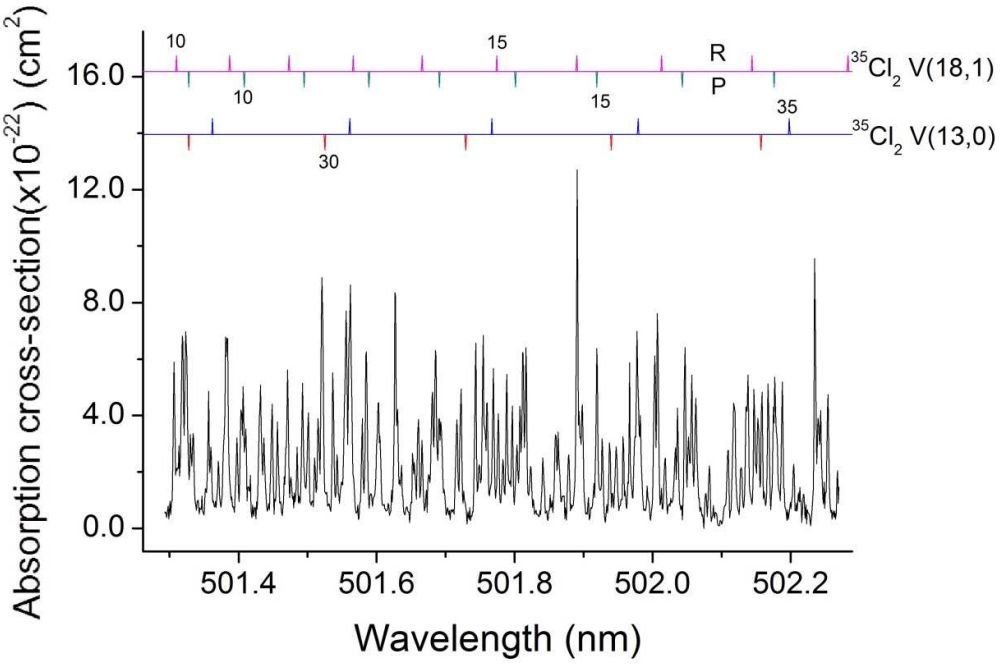

Fig.6

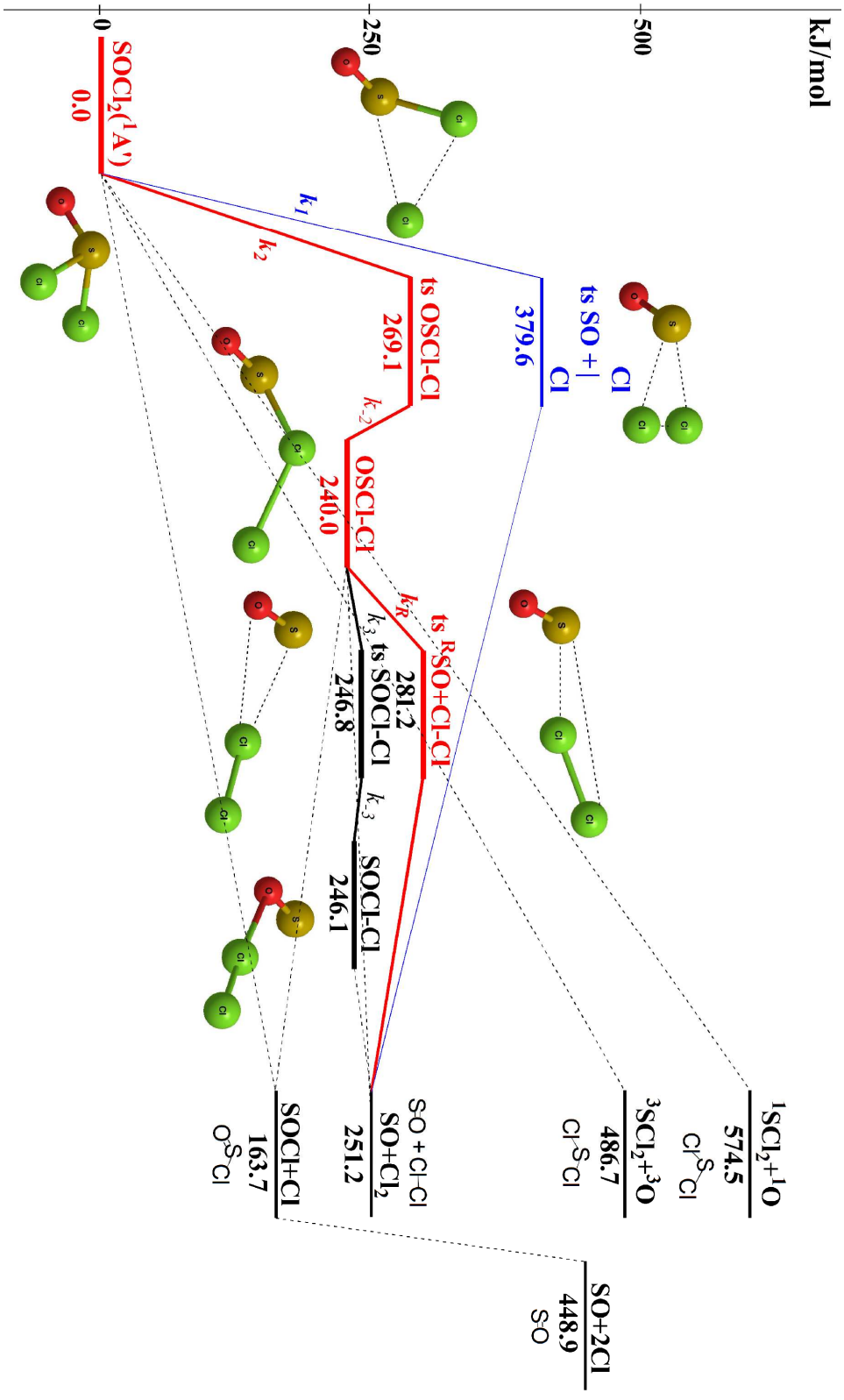

Fig.7

(a) reactant

$SOCl_2$ ($^1A'$, C_S)

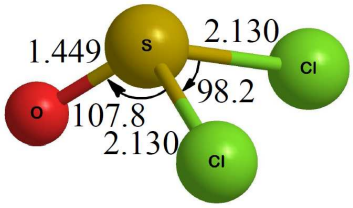

(b) intermediate

OSCl-Cl (^1A, C_1)

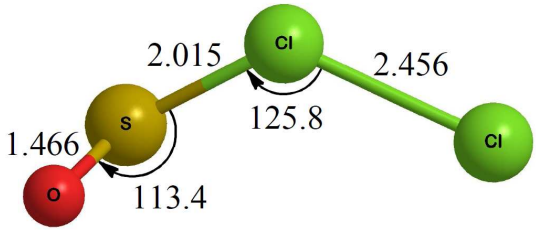

SOCl-Cl (^1A, C_1)

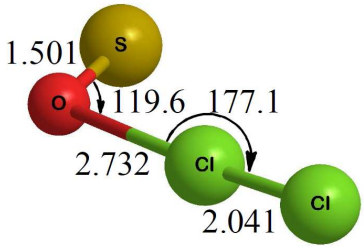

(c) molecular dissociation products

SO ($^1\Sigma$, $C_{\infty v}$)

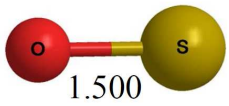

Cl_2 ($^1\Sigma_g^+$, $D_{\infty h}$)

(d) atomic dissociation products

SOCl ($^2A''$, C_S)

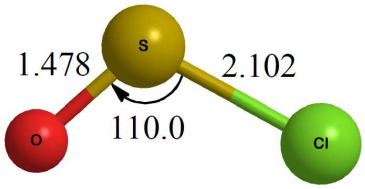

SCl_2 ($^1A_1$, C_{2V})

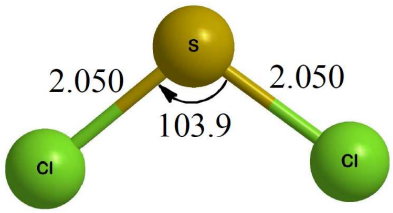

SCl_2 ($^3B_1$, C_{2V})

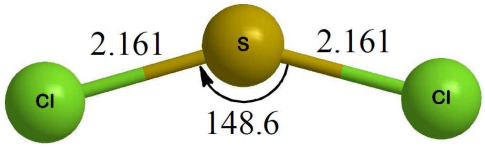

(e) transition states

ts$_{SO+Cl_2}$ (^{1}A, C$_1$)

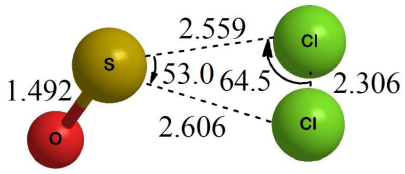

ts$_{OSCl\text{-}Cl}$ (^{1}A, C$_1$)

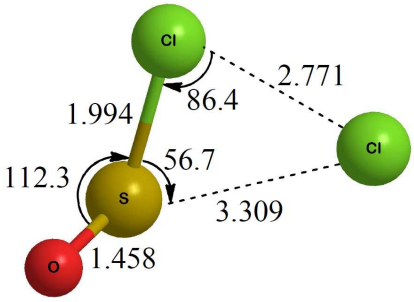

ts$_{SOCl\text{-}Cl}$ (^{1}A, C$_1$)

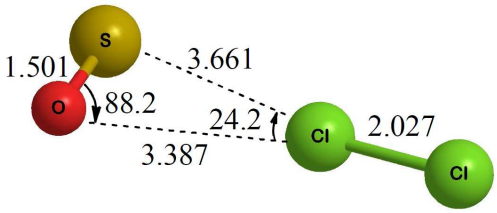

ts$_{R_{SO+Cl\text{-}Cl}}$ (^{1}A, C$_1$)

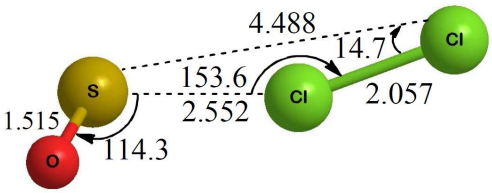

Fig.8

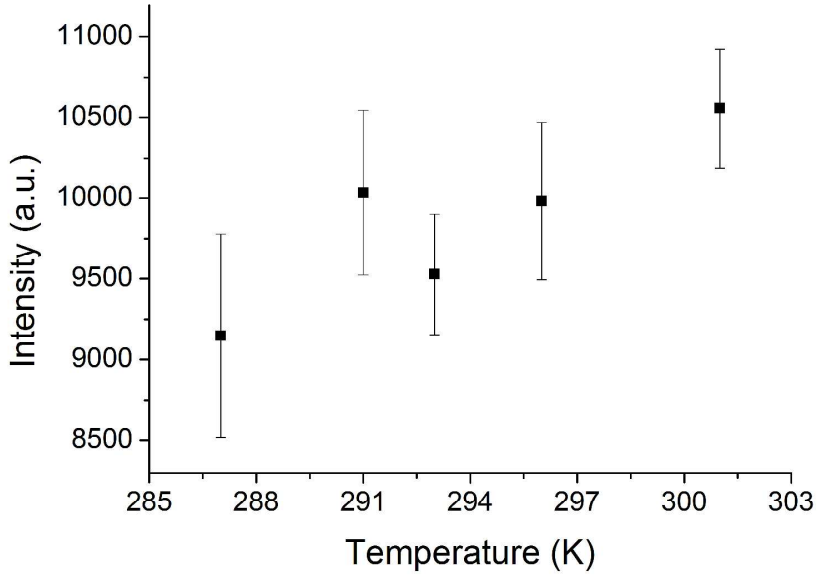

Fig.9